Oxidation behaviour of particle reinforced $MoSi_2$ composites at temperatures up to 1700 °C

Part III: Oxidation behaviour of optimised $MoSi_2$ composites

S. Lohfeld[1], M. Schütze[1]*, A. Böhm[2], V. Güther[3], R. Rix[3] and R. Scholl[4]

[1] Karl-Winnacker-Institut der DECHEMA e.V., Theodor-Heuss-Allee 25, D-60486 Frankfurt am Main (Germany)

[2] IFAM Dresden, Winterbergstr. 28, D-01277 Dresden (Germany)

[3] GfE Gesellschaft für Elektrometallurgie mbH, Höfener Str. 45, D-90431 Nürnberg (Germany)

[4] HC Starck GmbH, Kraftwerkweg 3, D-79725 Laufenburg (Germany)

Abstract

The topic "Oxidation behaviour of particle reinforced $MoSi_2$ composites at temperatures up to 1700 °C" is discussed in a three part publication. In the first part of this paper a literature survey on the oxidation behaviour of $MoSi_2$ and $MoSi_2$ composites has been given. In the second part an initial screening at 1600 °C revealed those composites which may be suitable for high temperature applications. The low temperature oxidation behaviour of selected composites in the "pest" region was examined as well. Additionally, the effect of iron impurities on the high temperature behaviour of the composites was explained. The present part deals with a detailed investigation of an optimised $MoSi_2/HfO_2$ composite. These investigations include high temperature oxidation at 1500 to 1700 °C and low temperature oxidation at 400 and 500 °C.

1 Introduction

In the previous parts of this publication a literature review [1] and an initial screening test [2] were used to check the suitability of selected $MoSi_2$ composites for high temperature applications. While in some cases limited oxidation resistance at 1600 °C of the material was expected due to formation of eutectics of the phases, the high temperature oxidation was seriously deteriorated by iron contamination. The series of composites were successively optimised and three composites containing SiC, ZrO_2 or HfO_2, respectively, were discovered to be most suitable for temperatures of 1600 °C and above. SiC composites have been investigated in detail in a separate work and are taken into consideration in the discussion section of the present paper. $MoSi_2$-HfO_2 composites showed a somewhat superior behaviour compared to $MoSi_2$-ZrO_2 composites so that optimisation was focused on the former. Further experiments were therefore carried out at temperatures up to 1700 °C to investigate the oxidation behaviour of the optimised $MoSi_2$-HfO_2 material in more detail and to obtain potential limitations of it.

2 Materials and methods

2.1 Materials

The optimized $MoSi_2$-HfO_2 composite investigated here was a composite containing 15% HfO_2 from production at a laboratory scale with a low iron contamination. Following the labelling introduced in part II of the present publication, the name of the series is I2, which stands for the second series from the manufacturer Fraunhofer IFAM. Characteristics of this series are given in Table 1.

Table 1: Sample series

Series	Reinforcement particles	Characteristics
I2	HfO_2	homogeneous, low Fe content, two series with hot pressing temperature of 1450 °C or 1550 °C, respectively

The two samples of this series were manufactured at different hot pressing temperatures, i.e. 1450 and 1550 °C, respectively. The corresponding specimens have been labelled I2a (1450 °C) or I2b (1550 °C).

The structures of the samples showed some distinctions: I2a was widely homogeneous, however, some large oxide precipitations have been found, Fig. 1, whereas I2b showed large areas depleted in HfO_2, see Fig. 2.

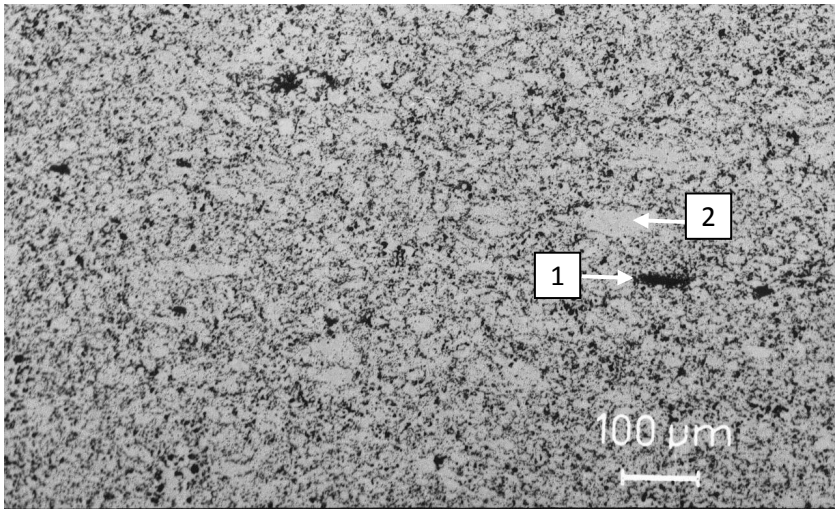

Figure 1: Cross section of $MoSi_2/HfO_2$ (series I2a):
widely homogeneous structure, single areas without HfO_2 (1) and coarse oxide precipitations (2)

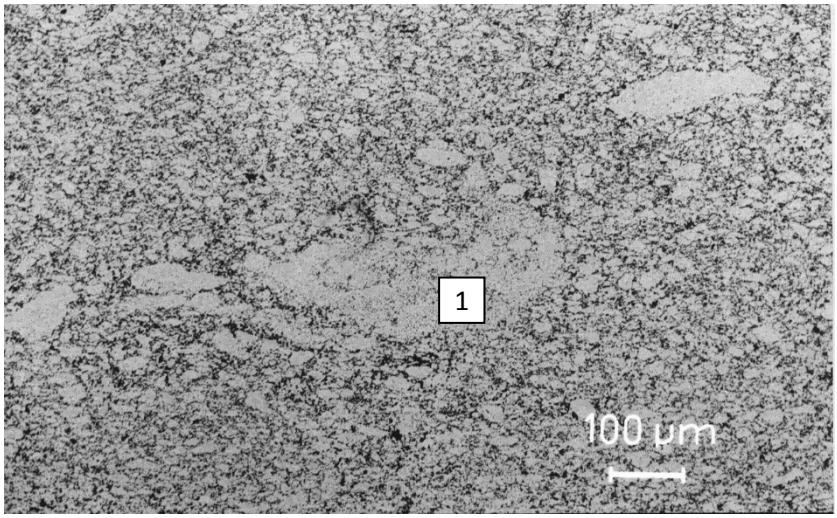

Figure 2: Cross section of $MoSi_2/HfO_2$ (I2b) with large areas depleted in HfO_2 (1)

2.2 Methods

All experiments and post experimental investigations were conducted following the description given in part II of this paper.

3 Results

Extended investigations were applied especially to the I2a specimens. Based on its homogeneous structure and low iron content this material is close to the expected final development stage. New labels are necessary for these specimens, since several tests were performed with identical samples. The specimens were distinguished by a letter following a number which indicates the oxidation temperature divided by 100, e.g., specimen 15.A is one of the samples oxidised at 1500 °C.

3.1 Oxidation at 1500 °C

Table 2 gives the mass changes of $MoSi_2/HfO_2$ after 30, 100 and 300 h exposure, respectively. Specimens 15.A and 15.B as well as 15.C to 15.E were each cut from the same bending sample. Note the discrepancy in mass changes between A and B compared to C to E. It was found that the latter had a higher density (6.3 versus 6.05 g/cm³). Primarily the mass gain within the first 30 h was very dissimilar, whereas following this period oxidation rates were nearly the same, Fig. 3.

Table 2: Mass changes of $MoSi_2/HfO_2$ (series I2a) after 30, 100 und 300 h oxidation at 1500 °C in air (in mg/cm²)

	15.A	**15.B**	**15.C**	**15.D**	**15.E**
30 h	1.112	1.002	0.392	0.345	0.394
100 h	1.186	1.296	0.607	--	0.568
300 h	--	1.508	--	--	0.832

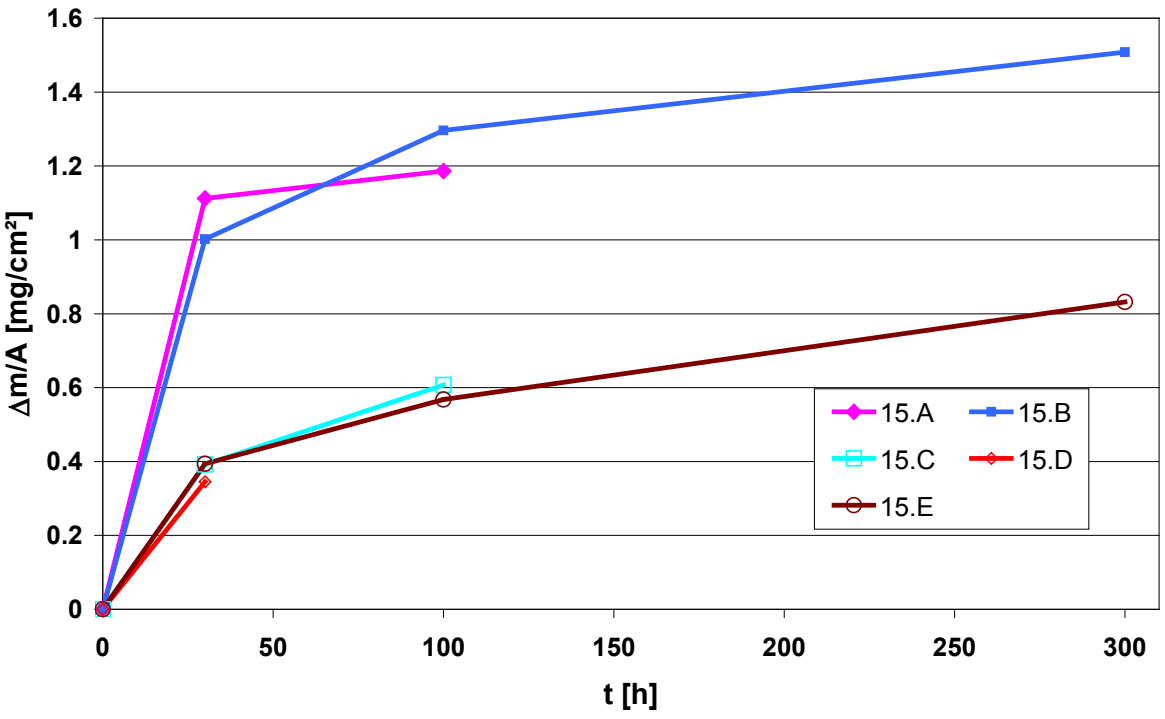

Figure 3: Mass change of $MoSi_2/HfO_2$ (series I2a) at 1500 °C

The lower density observed for specimens A and B can cause higher open porosity. Surface defects can have a significant influence in the first hours of oxidation, because the actual surface area is larger than measured. This would result in a higher calculated oxidation rate. This effect seems to be observed in case of specimens A and B.

Independently of the density the oxide layer thickness was 4 µm after 30 h, 5-10 µm after 100 h and 10 µm after 300 h.

3.2 Oxidation at 1600 °C

Despite of similar densities of specimens 16.A to 16.C and 16.D to 16.F, which again were each cut from one bending sample, as well as similar oxide layer thicknesses, mass changes varied partially strongly, see Table 3. The reason for this could not be determined exactly. Both restricted oxygen transport to the specimen support surface and an inhomogeneous second phase particle distribution could cause different mass gains. The summarised mass gain after 300 h was lower for oxidation at 1600 °C than it was at 1500 °C, due to the smaller increase within the first 30 h. Mass changes between 30 and 100 and between 100 and 300 h showed higher oxidation rates at 1600 °C compared to 1500 °C, see Fig. 4.

The oxide layer thickness was 4 µm after 30 h, 8 µm and 10 µm after 100 and 300 h, respectively, which was similar to the values obtained at 1500 °C.

There was no evidence of contact reactions with the HfO_2 supports, however, the oxide layer was less developed or not present in the contact area, see Fig. 5.

Table 3: mass change of $MoSi_2/HfO_2$ (series I2a) after 30, 100 and 300 h oxidation at 1600 °C in air (in mg/cm²)

	16.A	**16.B**	**16.C**	**16.D**	**16.E**	**16.F**
30 h	0.536	0.537	0.599	0.388	0.274	0.218
100 h	0.758	--	0.882	0.585	--	0.575
300 h	--	--	1.154	0.96	--	--

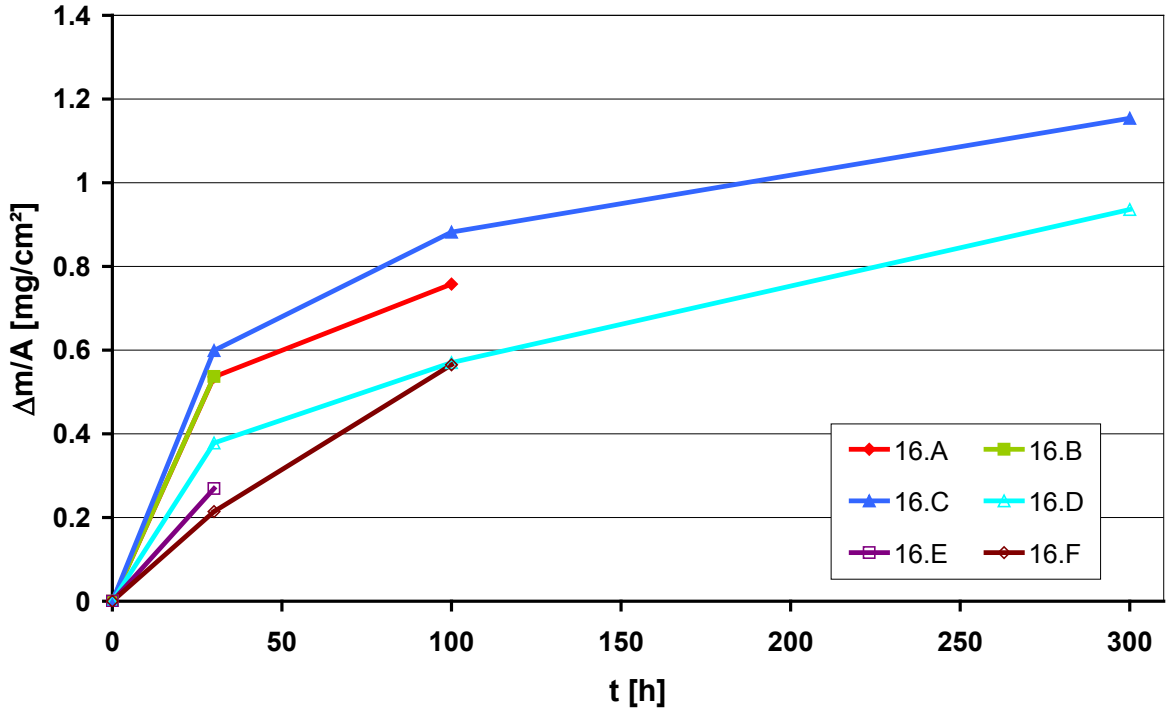

Figure 4: mass change of $MoSi_2/HfO_2$ (series I2a) at 1600 °C

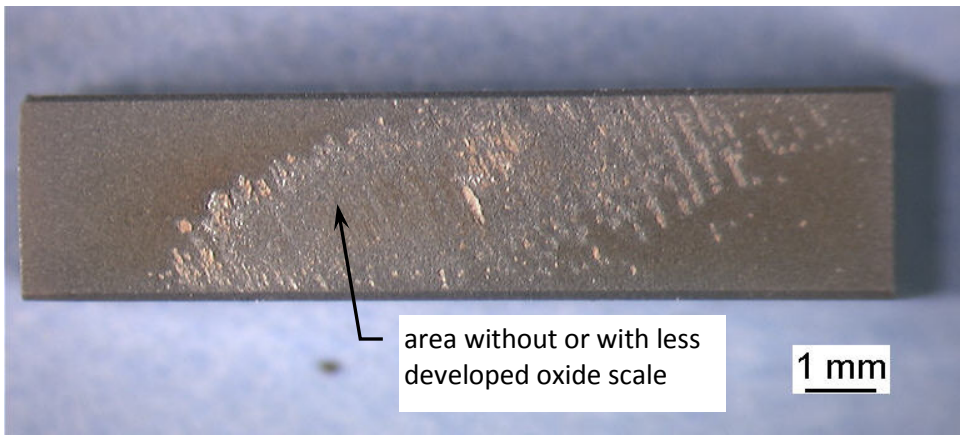

Figure 5: Support area of specimen 16.A ($MoSi_2/HfO_2$, series I2a) after 30 h at 1600 °C in air: reduced oxidation

Intensive agglomeration of hafnon particles occurred with increased oxidation duration. Whereas a homogeneous distribution was observed from a SEM image after 100 h, see Fig. 6, there were large dense packed areas of these particles after 500 h, see Fig. 7.

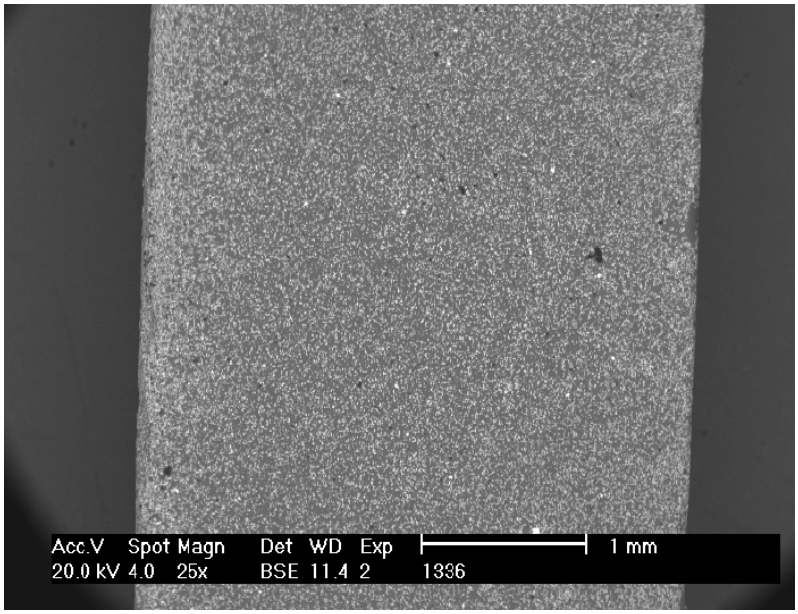

Figure 6: SEM image of $MoSi_2/HfO_2$ (series I2a) after 100 h at 1600 °C in air: homogeneous distribution of hafnon particles

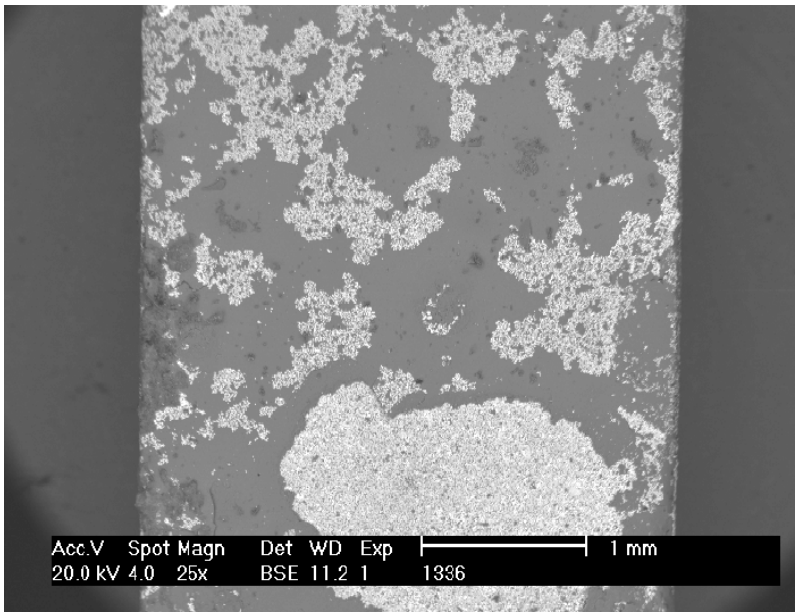

Figure 7: SEM image of $MoSi_2/HfO_2$ (Series I2a) after 500 h at 1600 °C in air: Agglomerated hafnon particles

3.3 Oxidation at 1700 °C

To avoid the observed reduced oxidation at the contact surface, the supports were given a shape that provides line contact with the specimens.

A very irregular oxidation behaviour of the specimens occurred in this test, although all specimens were cut from the same bulk material. Three out of six specimens were damaged after 30 h by formation of big bubbles in the oxide scale, Fig. 8. After cooling a powdered substance was discovered in the affected areas, see Fig. 9. The remaining three specimens (17.B, 17.C and 17.F) had largely

undamaged oxide scales and increased masses. Only tiny bubbles causing the loss of the oxide scale were found on the small areas, though the integrity of the material was unaffected. Two of these specimens were oxidised additional 70 h, whereto they were defective as well, see Fig. 10. The SEM image on the right side of Fig. 11 shows MoO_3 crystals in the powder on the specimens.

The test was repeated with two more specimens (17.G and 17.H), which again showed diverse behaviour. It is believed that the material used for these specimens originated from varied lots. 17.G was cut from the bulk material already used for 17.A to 17.F, whereas 17.H was part of a specimen prepared for a bending test. This sample had a higher density (6.3 instead of 6.1 g/cm^3).

At 1700 °C mass gains were significantly higher than at 1600 °C: between four and twenty times as high after 30 h, see Table 4.

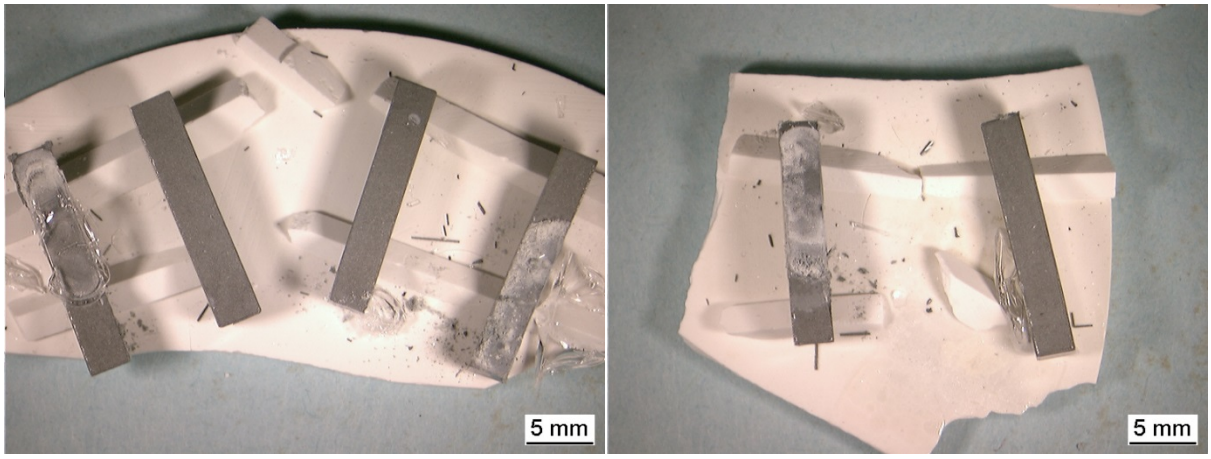

Figure 8: $MoSi_2/HfO_2$ (series I2a) after 30 h at 1700 °C in air: formation of big “glass” bubbles on three out of six specimens and spallation of edges

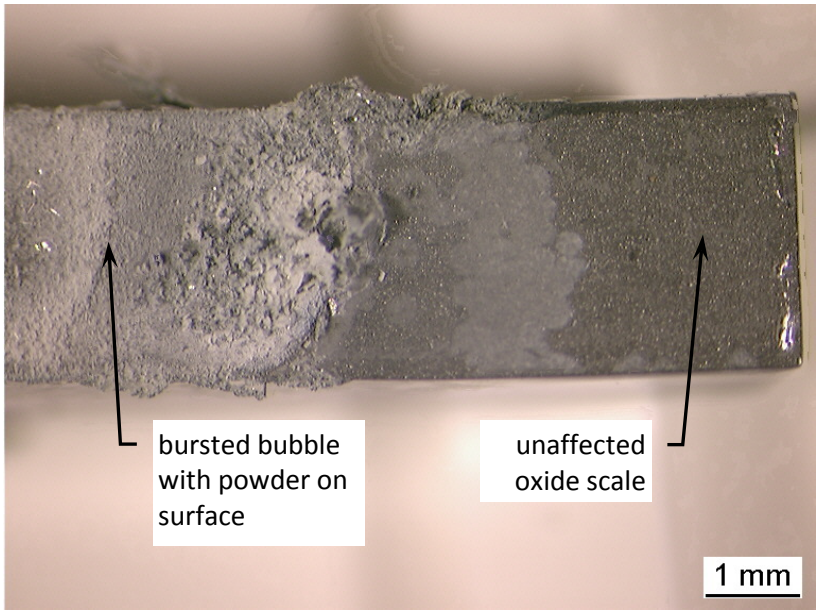

Figure 9: $MoSi_2/HfO_2$ (series I2a) after 30 h at 1700 °C in air: left side: powder beneath bursted bubble, right side: undamaged oxide scale

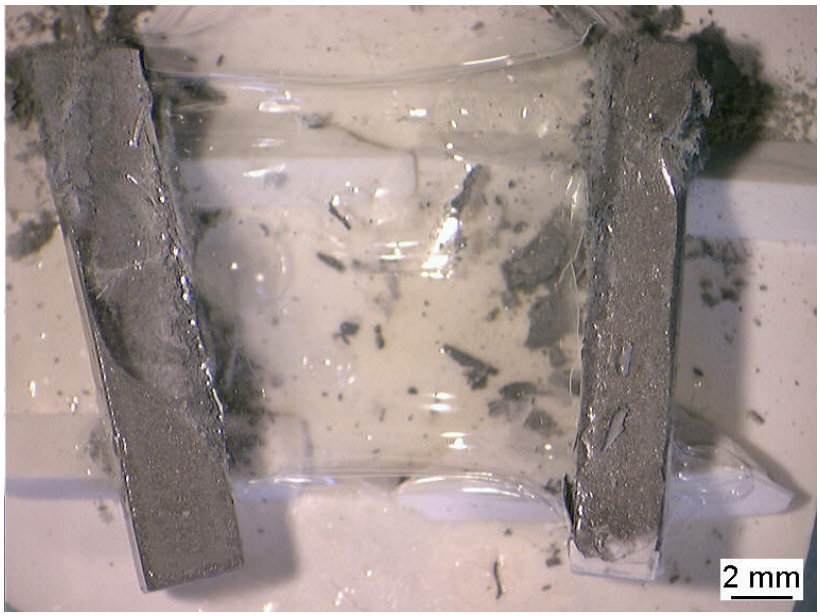

Figure 10: $MoSi_2/HfO_2$ (series I2a) after 100 h at 1700 °C in air: collapsed bubble connecting the specimens

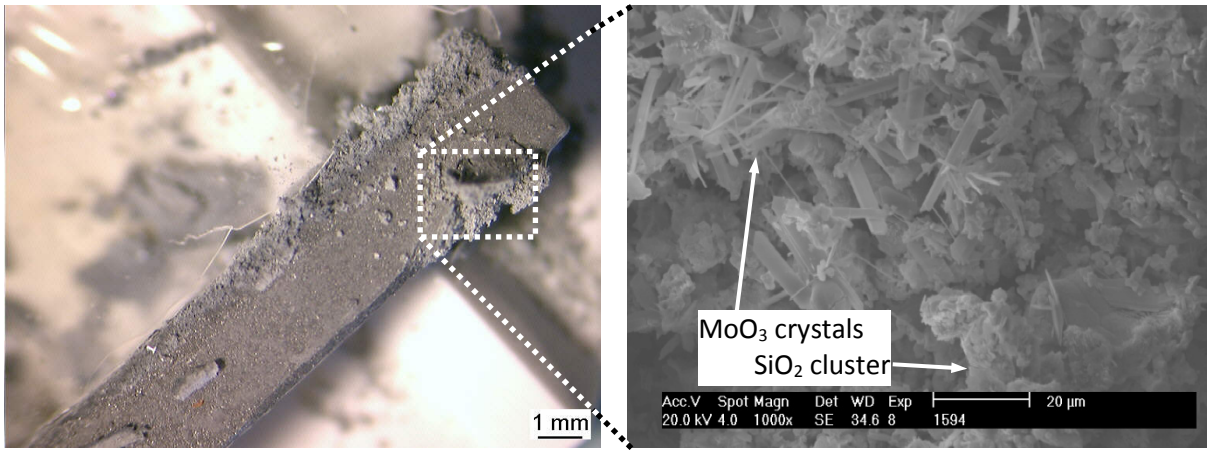

Figure 11: $MoSi_2/HfO_2$ (series I2a) after 100 h at 1700 °C in air: crystals of MoO_3 were identified in the powder on the specimens

Table 4: Mass change of $MoSi_2/HfO_2$ (series I2a) after 30 and 100 h oxidation at 1700 °C in air (in mg/cm²)

	17.A	**17.B**	**17.C**	**17.D**	**17.E**	**17.F**	**17.G**	**17.H**
30 h	-0.112	4.184	2.144	-12.325	-6.517	4.328	-19.415	0.968
100 h	--	-12.399	-22.78	--	--	--	--	--

In Fig. 12 the remnants of a bubble above a cavity are visible. It is assumed that the cavity leads to an accumulation of Mo_5Si_3, which was detected in several composites investigated. From sites like this one larger amounts of molybdenum oxide can form.

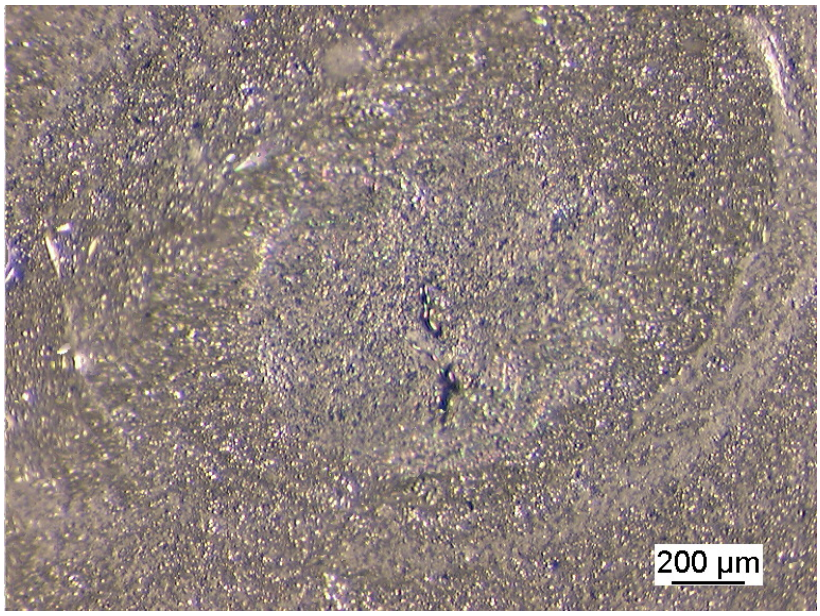

Figure 12: $MoSi_2/HfO_2$ (series I2a) after 100 h at 1700 °C in air: bursted bubble above cavity

No contact reactions with the HfO_2 supports occurred, however, the supports contacting edge stuck to the oxide scale in some cases. During cooling some edges of the specimens spalled off. Due to spallation and evaporation of gaseous products mass changes do not solely result from oxide scale growth.

3.4 Continuous thermogravimetric investigations at 1500 °C

Three measurements for the $MoSi_2/HfO_2$ composite revealed rapid mass gain at the beginning of oxidation and lower growth rates after formation of a dense SiO_2 scale after 5-10 h, see Fig. 13. Mass loss as it is usually observed for pure $MoSi_2$ at the beginning of oxidation occurred in one test only and was rather small.

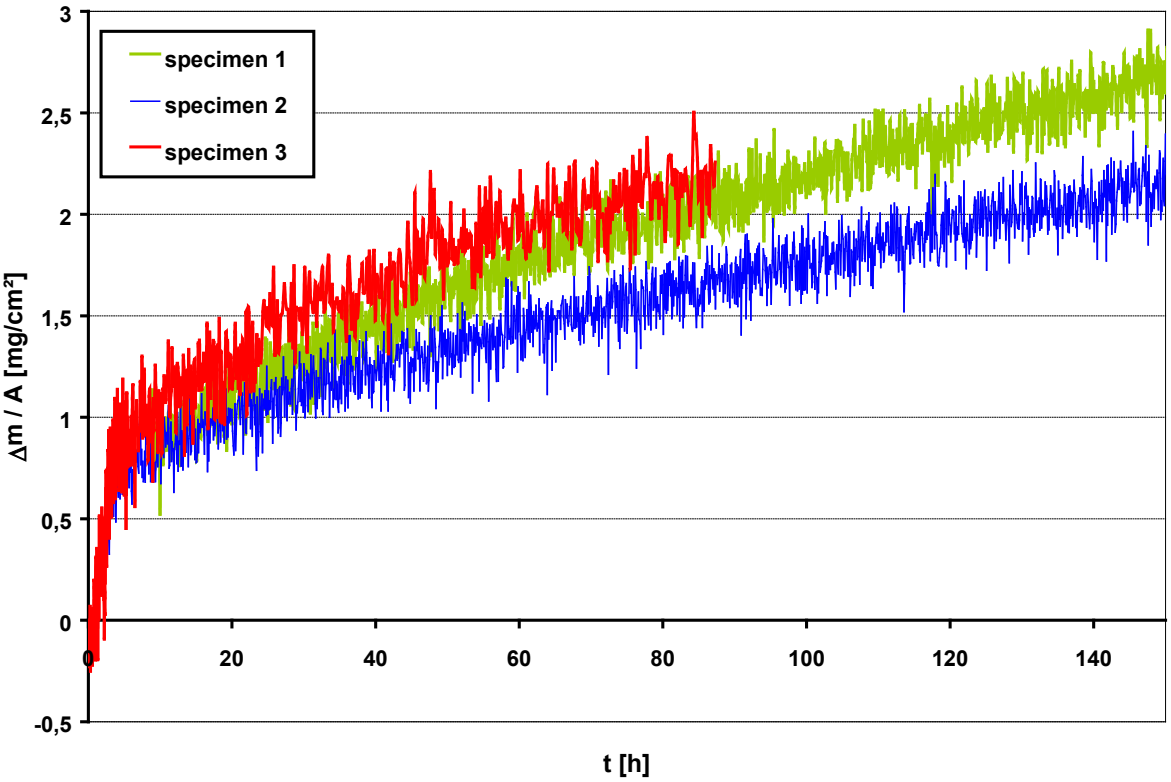

Figure 13: Mass change as a function of time at 1500 °C in air for $MoSi_2/HfO_2$ (series I2a)

3.5 Oxidation at "pesting" temperatures

Two specimens each of type I2a, I2b and pure $MoSi_2$ were oxidised at 400 °C. One of each type was preoxidised for 70 h at 1400 °C in air to detect the influence of preoxidation. Fig. 14 shows the specimens after 575 h oxidation. The I2b specimen without preoxidation disintegrated completely, the powder covered some other specimens.

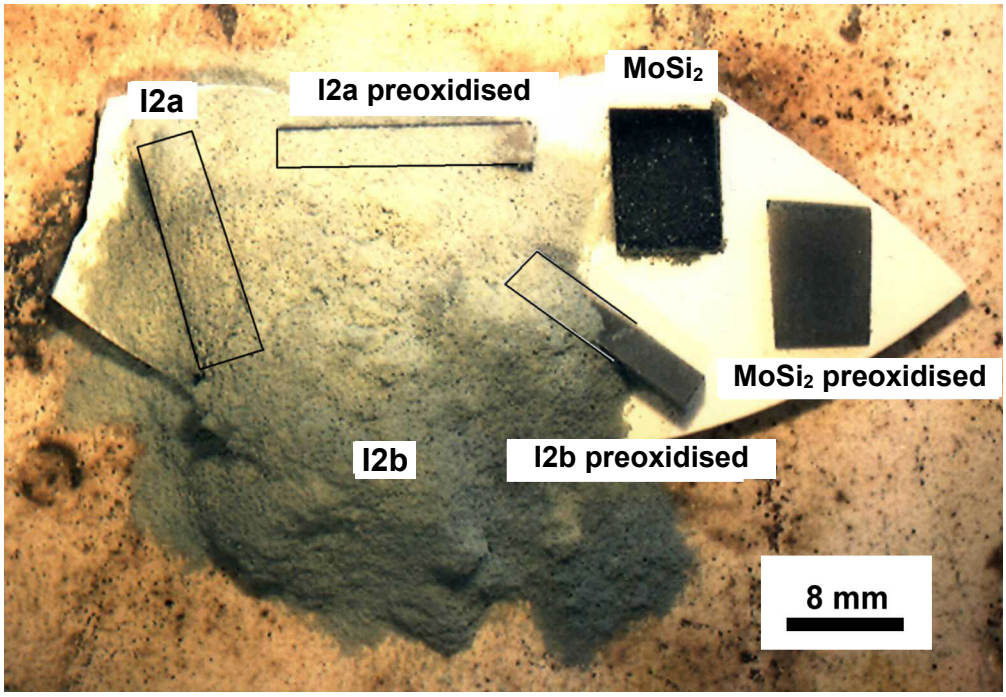

Figure 14: $MoSi_2/HfO_2$ (series I2) and pure $MoSi_2$ after 575 h at 400 °C in air: Complete disintegration of I2b specimen without preoxidation (position of specimens covered by powder is indicated by lines)

Specimens without preoxidation

Green-yellowish crystals formed after 90 h on the composites. Pure $MoSi_2$ had a dull black surface with white oxidation products like observed on $MoSi_2$/SiC (series G4) in ref. [2] after 500 h at 500 °C. After 250 h specimen I2b cracked into three parts and MoO_3 formed on this and on the I2a specimen. Pure $MoSi_2$ showed MoO_2 crystals at the edges. Disintegration of I2b was nearly complete after 300 h. I2a was covered with a dense layer of crystals, however, no cracking occurred. Pesting seemed to be limited to the surface region. No further changes were observed for pure $MoSi_2$.

A second test was performed at 500 °C. After 100 h the surfaces appeared black, subsequently a thin yellowish layer formed, Fig. 15. No disintegration or cracking happened within 500 h testing time.

Figure 15: Macroscopic view of $MoSi_2/HfO_2$ (series I2b) after 500 h at 500 °C in air: thin yellow layer consisting of MoO_3 crystals and SiO_2 clusters

Preoxidised specimens

Minor damage in small areas of the oxide scale was observed for the preoxidised specimens. Fig. 16 shows spots of white powder found after 250 h. A brown oxide scale occurred on pure $MoSi_2$ after 90 h and has turned dark green when the test was finished. The white spots on the composites grew slightly until the end of the test.

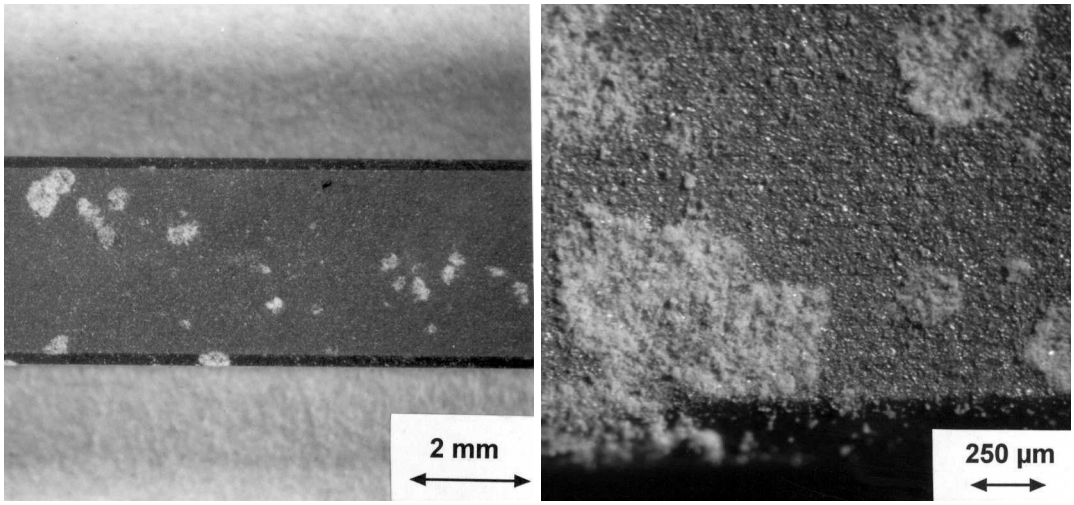

Figure 16: Preoxidised $MoSi_2/HfO_2$ (series I2a) after 575 h at 400 °C in air: occasional spots with white powder (right side: magnified view)

No disintegration was observed when these specimens were subsequently oxidised for another 500 h at 500 °C. The white spots increased insignificantly in size and some MoO_3 was found on pure $MoSi_2$.

4 General discussion and conclusions of the paper (including findings of parts I and II)

4.1 High temperature oxidation

4.1.1 Oxidation of pure $MoSi_2$

At high temperatures a dense SiO_2 scale forms quickly and hinders the formation of MoO_3 by lowering the oxygen partial pressure. Fig. 17 shows that at low oxygen partial pressures MoO_3 will not form.

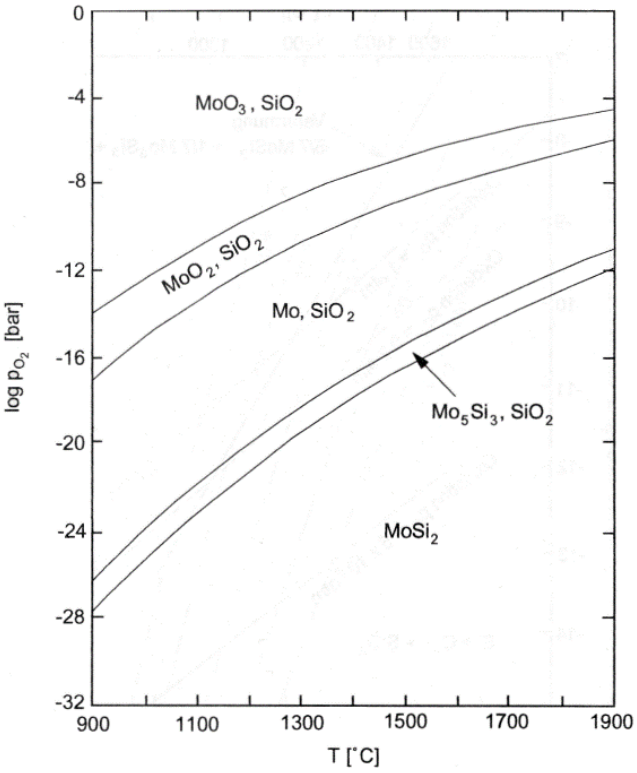

Figure 17: Thermodynamic stability of the condensed phases in the system Mo-Si-O [3]

Therefore, above 1000 °C $MoSi_2$ will transform into Mo_5Si_3 while SiO_2 originates in the selective oxidation of silicon following equation (1). MoO_3 cannot evaporate if the specimen is sealed with SiO_2, and a layer of Mo_5Si_3 will form beneath the oxide scale. Otherwise Mo_5Si_3 would oxidise to MoO_3 and SiO_2 according to equation (2).

$$5\ MoSi_{2\,(s)} + 7\ O_{2\,(g)} \rightarrow Mo_5Si_{3\,(s)} + 7\ SiO_{2\,(s)} \quad (1)$$

$$2\ Mo_5Si_{3\,(s)} + 21\ O_{2\,(g)} \rightarrow 10\ MoO_{3\,(g)} + 6\ SiO_{2\,(s)} \quad (2)$$

However, Melsheimer [4] and Bundschuh [5] observed that no layer of Mo_5Si_3 is formed at high temperatures (1500 °C), because molybdenum diffuses through the SiO_2 scale and oxidises to MoO_3 at the surface. In the present work the specimens oxidised at 1600 °C not only showed no Mo_5Si_3 in the metal boundary layer, but all Mo_5Si_3 in this region which was observed prior to oxidation disappeared as well. An accelerated diffusion of molybdenum, occurring because phase boundary diffusion is enhanced by the second phase particles, prevented the formation of a Mo_5Si_3 layer.

4.1.2 General considerations on the influence of second phases

The oxide scale on $MoSi_2$ grows inward since diffusion of oxygen in SiO_2 is faster than that of silicon [4]. Within the oxide scale the oxidic second phase particles react with SiO_2 to form silicates gathering at the surface. For example traces of zirconium found in the oxide scale of $MoSi_2/ZrO_2$ indicated some solubility in SiO_2 as well as diffusion causing the gathering of particles at the surface. Small particles also coagulated in the core-area of the material to form large ones, combined with growing matrix grains. Hence, modified mechanical properties are most likely. Neither matrix grain growth nor a coarser particle distribution was observed for the $MoSi_2$/SiC composite, making this one more suitable for high temperature applications.

As perceived in series I1, oxidation rates of the composites increased moderately compared to pure $MoSi_2$. Second phases permit faster oxygen transport to the $MoSi_2/SiO_2$ interface because they widen the SiO_2 network.

Lower mass gains for the oxidic and carbidic reinforced composites of series G2 compared to series I1, though the scale thicknesses were slightly higher, were due to evaporation of MoO_3. The surplus of molybdenum coming from the mill caused a higher amount of Mo_5Si_3 in the materials, which is preferably oxidised to MoO_3. The series of boridic reinforced composites cannot be compared since their structures and phases originating from different manufacturing routes were totally different. The high amount of SiO_2 in the boridic reinforced composites of series G2 and G3 results from the usage of MoO_2 and ZrB_2 or HfB_2, respectively, when producing the sinterpowders. Thermodynamic calculation showed that these phases react according to equation (3), while in absence of MoO_2 only Mo and Si react to form $MoSi_2$, see equation (4). Considering atmospheric oxygen, the formation of SiO_2 is thermodynamically possible, however, the other reaction products in equation (5) were not found in the material, indicating that no reaction with atmospheric oxygen had happened.

$$Mo + 12\,Si + 5\,MoO_2 + 2\,ZrB_2 \rightarrow 4\,MoSi_2 + 2\,MoB + 3\,SiO_2 + ZrB_2 + ZrSiO_4 \quad (3)$$

$$Mo + 2\,Si + ZrB_2 \rightarrow MoSi_2 + ZrB_2 \quad (4)$$

$$Mo + 2\,Si + ZrB_2 + 6\,O_2 \rightarrow MoO_3 + SiO_2 + B_2O_3 + ZrSiO_4 \quad (5)$$

4.1.3 Thermogravimetric measurements

Unlike pure $MoSi_2$ the $MoSi_2/HfO_2$ composite revealed a significant mass gain right from the start of oxidation, turning into parabolic growth over the course of the test. Compared to pure $MoSi_2$ and ZrB_2 and ZrB_2/SiC reinforced $MoSi_2$ mass gain was accelerated in the first hours of oxidation and kept the pace of mass gain of the $MoSi_2/ZrB_2$/SiC composite thereafter, see Fig. 18. The surface was quickly sealed by the growing SiO_2 scale, decelerating oxygen transport and slowing down mass gain. Mass loss due to evaporating MoO_3 did not occur. This can be explained by a smaller affected surface area (15% less when particles are distributed ideally) and a faster growing oxide scale. Bundschuh et al. measured no initial mass loss for $MoSi_2$/SiC composites when the amount of SiC was sufficiently high and explained this with the formation of a dense SiO_2 scale from SiC particles [6]. In case of the HfO_2 reinforced $MoSi_2$ composite the mentioned accelerated diffusion of oxygen caused rapid sealing of the surface and a high oxidation rate throughout the testing time, see Fig. 19. A higher mass gain for ZrO_2 and HfO_2 reinforced $MoSi_2$ composites compared to $MoSi_2$/SiC was also confirmed in discontinuous tests at 1600 °C in air.

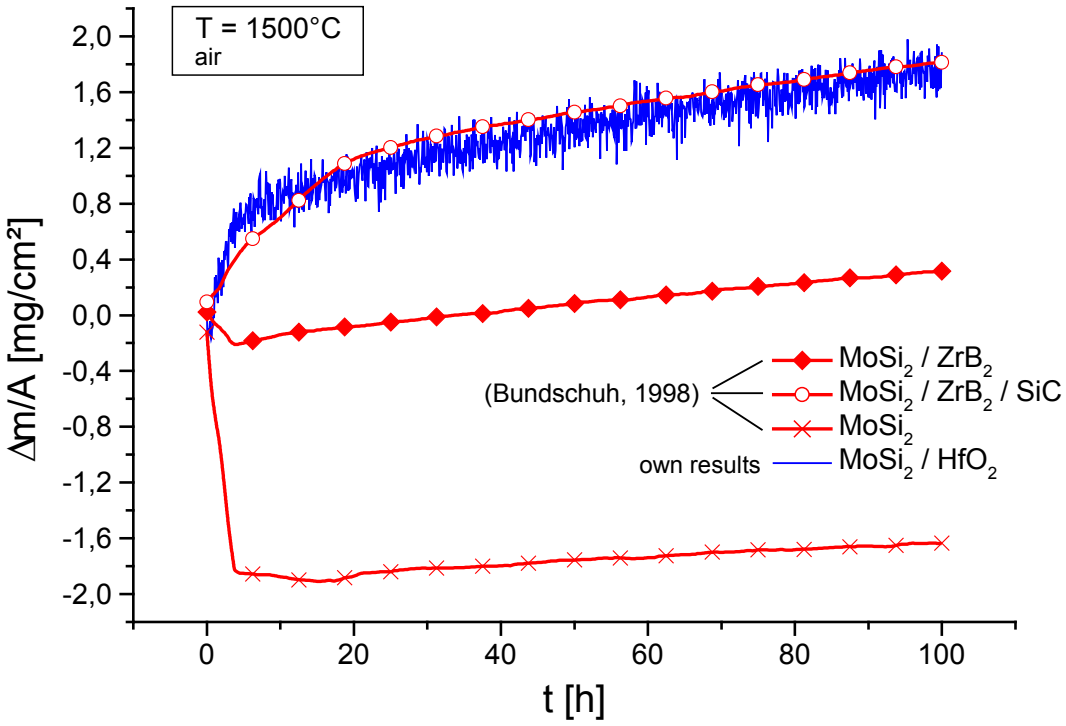

Figure 18: Mass change as a function of time for several $MoSi_2$ composites at 1500 °C in air

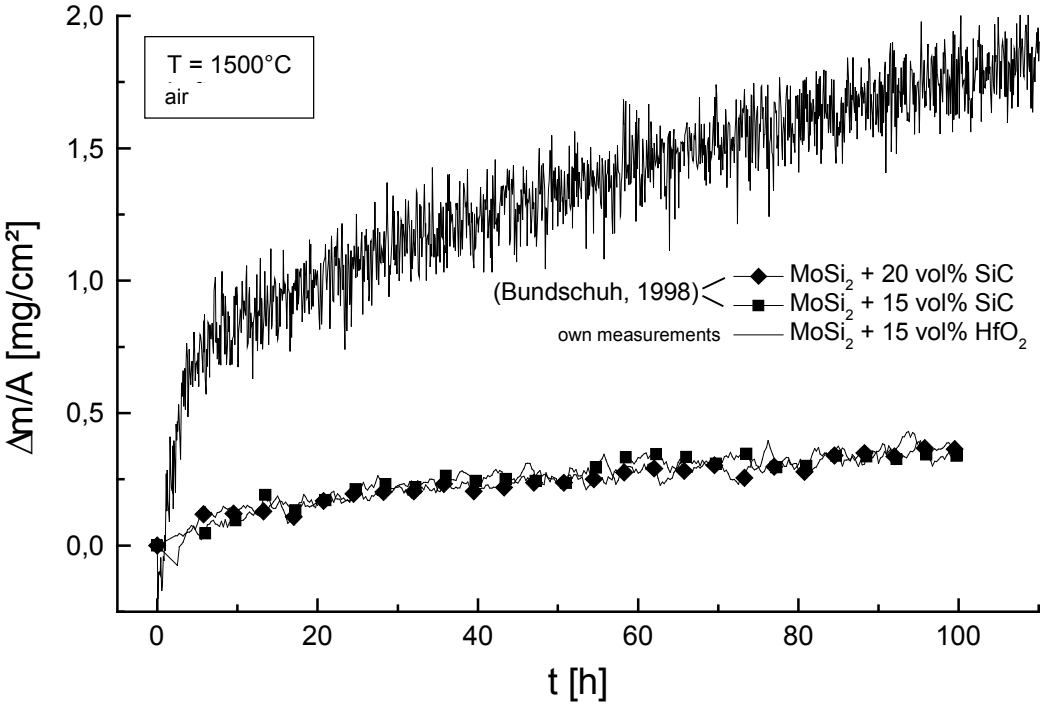

Figure 19: Mass change as a function of time for $MoSi_2/HfO_2$ compared to $MoSi_2/SiC$ at 1500 °C in air

The characteristics of oxidation kinetics did not change at higher temperatures. Several factors must be taken into account for explaining the same scale thickness but lower mass gain at 1600 °C versus 1500 °C during the first 30 hours of oxidation:

1) The diffusion rate of Mo in SiO_2 increased with the higher temperature and with a lower viscosity of the oxide scale. That means that more MoO_3 will evaporate, leading to higher mass loss. The rather short path of diffusion within the first hours facilitates rapid evaporation.
2) Bottleneck pores and pits will be closed quickly when the oxide scale growth rate is high and the viscosity is low. The actual surface area will rapidly match the geometric one, giving a "true" oxidation rate, whereas in the other case the area used to calculate the rate is actually larger than assumed, leading to lower rates. Fig. 20 facilitates understanding of this process.
3) The specimens had a larger support surface with reduced oxygen supply and impeded oxide scale growth. The estimated oxidised surface is larger than the actual one, resulting in a lower calculated growth rate.

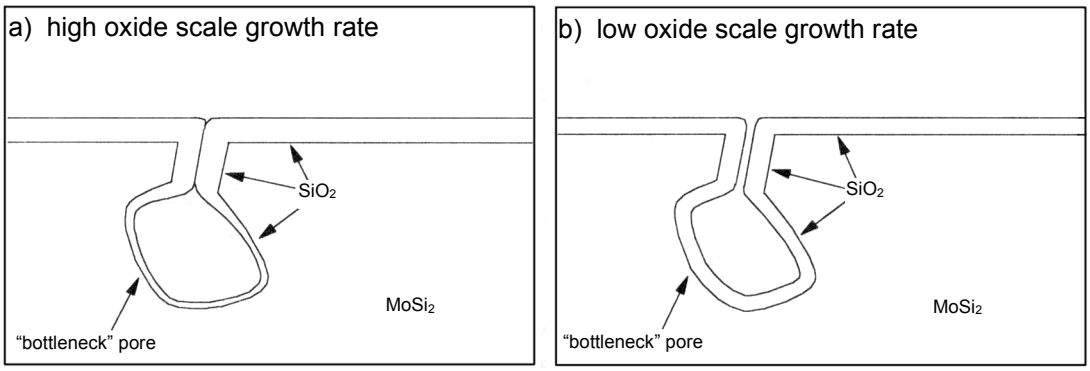

Figure 20: Sealing of the surface at different oxide scale growth rates:
a) high growth rate, fast closure of bottleneck pores, no further oxidation within the pore
b) low growth rate, slow oxide scale growth at necks of pores enable further oxidation within the pore

Long oxidation tests with more than 100 h duration revealed slightly higher oxidation rates at elevated temperatures due to accelerated diffusion. The slope of the mass gain curves is a little steeper for 1600 °C than for 1500 °C, see Fig. 21.

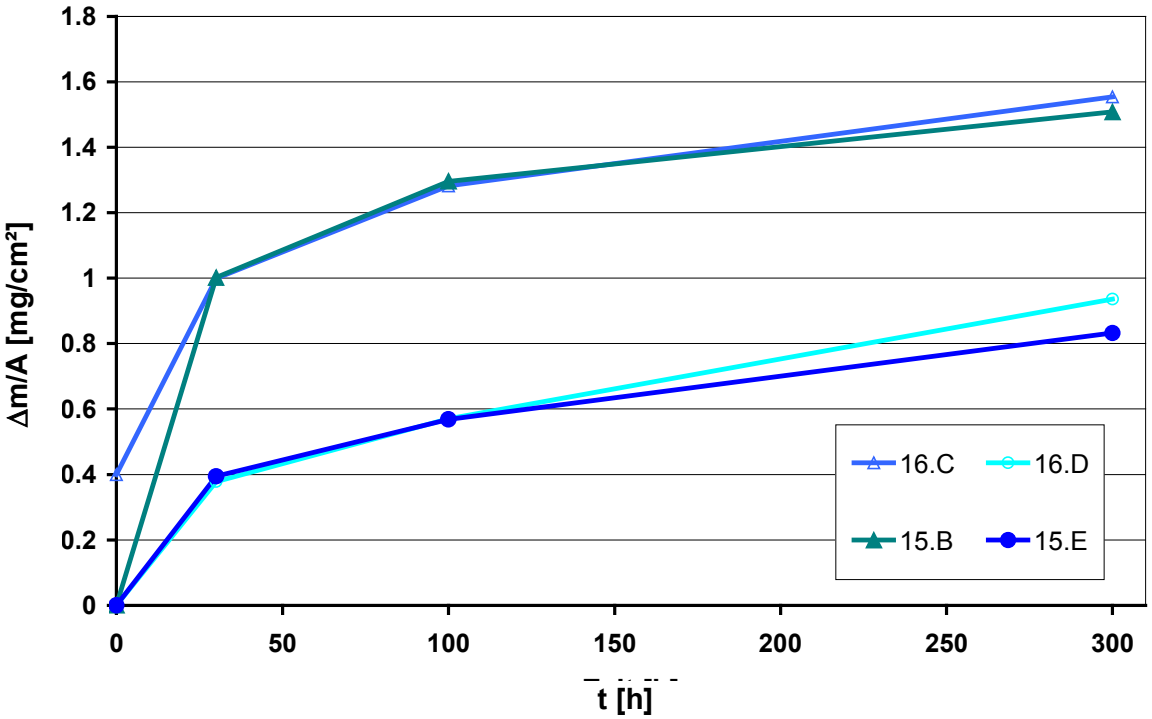

Figure 21: Comparison of oxidation kinetics (slopes after initial oxidation) of $MoSi_2/HfO_2$ at 1500 °C (two specimens labelled 15.B and 15.E) and 1600 °C (two specimens labelled 16.C and 16.D). The curve of specimen 16.C was shifted on the y-axis to allow comparison with curve 15.B with regard to the slope

Raising the furnace temperature to 1700 °C, the threshold of 1680 °C for formation of the eutectic phase of the system SiO_2-HfO_2 is surpassed and with liquid phases the oxidation accelerates drastically. The $HfO_2/MoSi_2$ composite is there therefore not suitable for applications with temperatures of 1700 °C and higher. Although time to failure was not always within 30 h, all specimens failed for the same reason. Bubbles were formed by evaporation of gaseous MoO_3. During cooling, smaller parts of the specimens spalled off and a powder had formed.

The precondition for bubble formation is a higher pressure within the bubble than the ambient pressure. The boiling point of MoO_3 is at 1155 °C. Fig. 22 shows that at 1700 °C the vapour pressure of MoO_3 is more than 2.6 bar. However, for technical applications the vapour pressure should not exceed 10^{-4} bar, where evaporation leads to measurable mass losses and reduction of the cross section [7]. Added vapour pressures of silicon oxides and MoO_2, being around 10^{-6} at 1700 °C, increase the value of 2.6 bar even further.

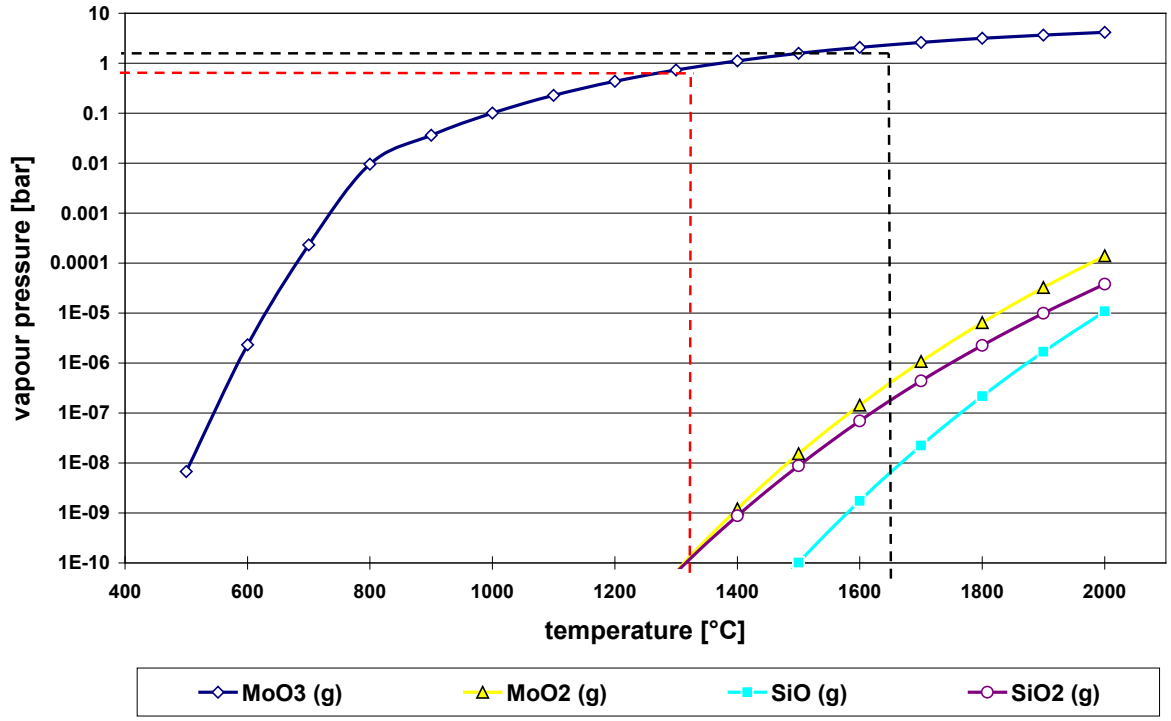

Figure 22: Calculated vapour pressures of gaseous oxides of molybdenum and silicon as a function of temperate at an oxygen partial pressure of 0.2 bar

To obtain pressures of more than the atmospheric pressure of 1 bar high amounts of MoO_3 are necessary. Since MoO_3 is primarily formed from Mo_5Si_3, these precipitations which occurred in the delivered material play an important role.

Fig. 23 facilitates understanding of the bubble formation. Prior to oxidation precipitations of Mo_5Si_3 exist in the subsurface area. During oxidation a layer of SiO_2 is formed. The SiO_2 scale grows at its inner interface, moving towards the Mo_5Si_3. Reached by the layer, Mo_5Si_3 is oxidised to a high concentration of MoO_3 below the SiO_2 scale. While at this very high temperature oxygen for this oxidation is delivered quickly through the scale, MoO_3 cannot diffuse fast enough outwards. The pressure causes the formation of a bubble in the scale with low viscosity. Fig. 24 shows such a bubble in the SiO_2 scale. The element distribution of Mo proves residues of the Mo-rich phase Mo_5Si_3 at the edge of the bubble. HfO_2 surface particles can even accelerate transport of oxygen to the Mo_5Si_3, causing its oxidation to SiO_2 and gaseous MoO_3. SiO_2 again reacted with HfO_2 to form $HfSiO_4$, which is now detected directly above and below the bubble. Aluminum in the oxide scale results from evaporation from the furnace chamber surface and enhances the diffusion rate of oxygen through the layer.

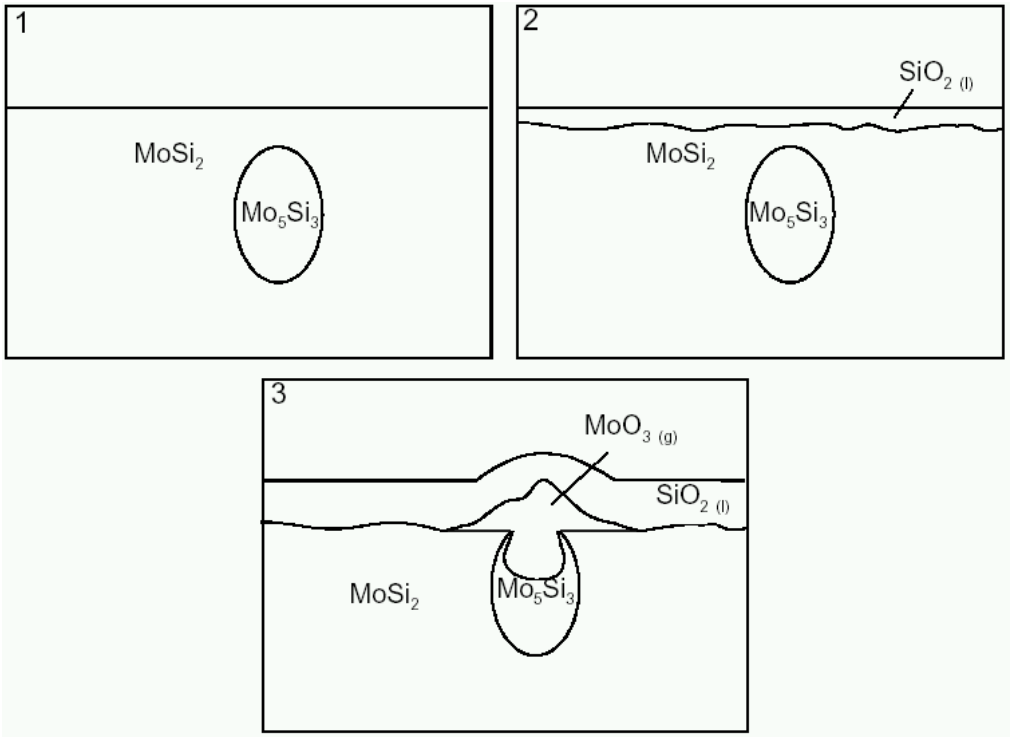

Figure 23: Bubble formation through oxidation of Mo_5Si_3

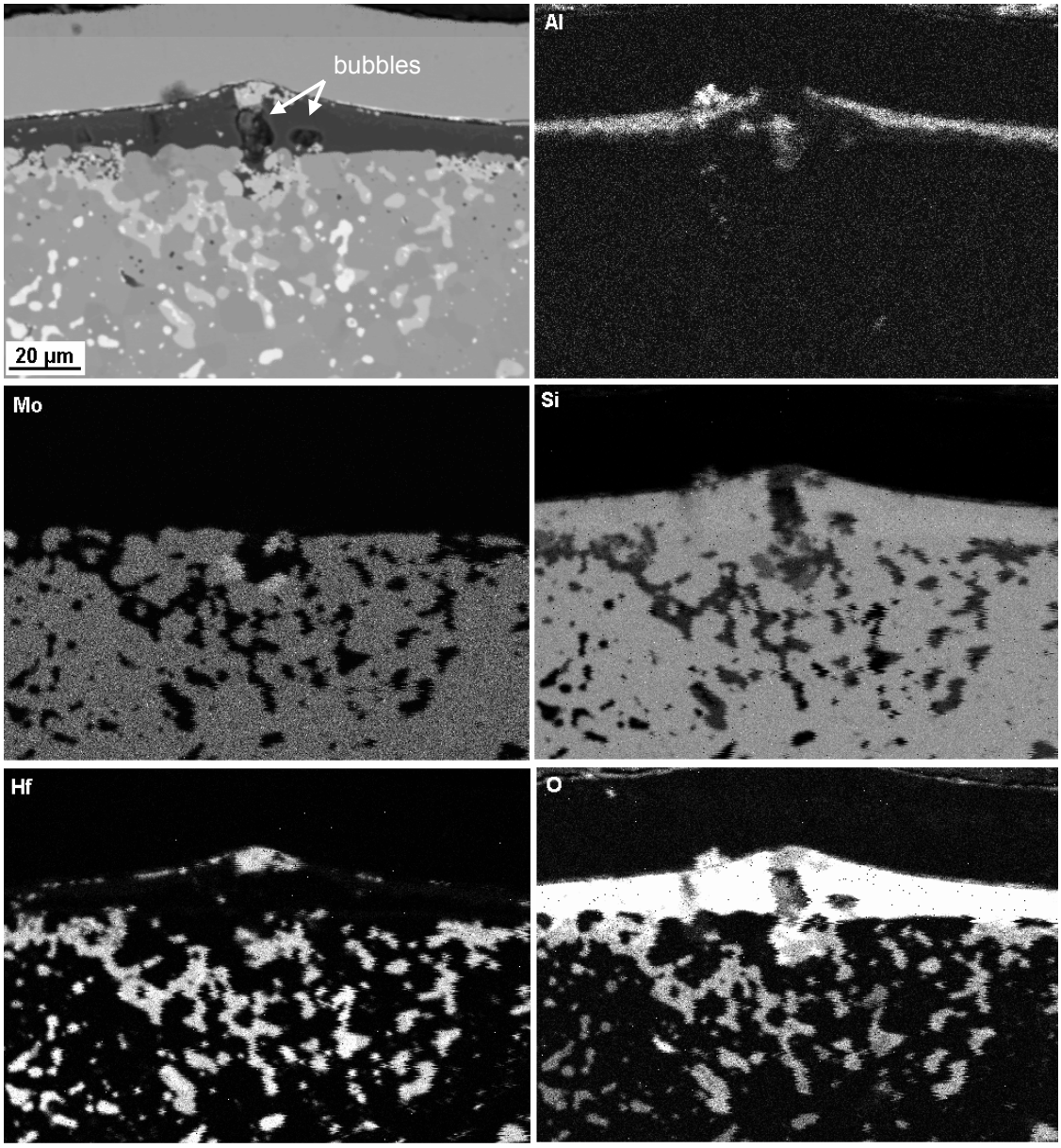

Figure 24: Back scattered electrons image and element distribution maps of $MoSi_2/HfO_2$ (series I2a) after 300 h oxidation at 1600 °C in air

Fig. 12 shows that the process described can produce holes in the material. Bubble formation was observed chiefly at very high temperatures, as oxygen transport to oxidise high amounts of Mo_5Si_3 is sufficient and scale viscosity is low enough, nevertheless it occurred in a smaller degree at 1600 °C as well.

In case the bubbles did not burst, the gaseous MoO_3 condensed during cooling and a layer of MoO_3 remained on the material, just like in the pesting tests. When the gas condensed in pores, the voluminous crystals led to stresses, cracking and spallation of the material.

Spallation of some edges during cooling might result from the slightly higher thermal expansion coefficient of cristobalite versus $MoSi_2$ ($\alpha_{cristobalite} = 10.3*10^{-6}\ K^{-1}$, $\alpha_{MoSi_2} = 8.5*10^{-6}\ K^{-1}$). In addition, the modification of cristobalite changes from a to the low temperature modification b between 270 and

200 °C, combined with a decrease in volume of 1.9 to 2.7% [9]. Both occurrences bring tension into the scale. Since this kind of spallation did not occur at 1600 °C and since the affected area is rather small, the stresses seem to be only slightly above the critical value.

4.2 Oxidation at "pesting" temperatures

The composite $MoSi_2/HfO_2$ of series I2 revealed the relation of pesting to the microstructure. Disintegration occurred for the specimen pressed at 1550 °C but not for that pressed at 1450 °C. The density for the latter was determined to be higher. The lower density indicates more pores and microcracks, where pesting generally begins.

Second phase particles could enhance pesting of $MoSi_2$ since oxygen diffuses more quickly at phase boundaries than through the volume. Additionally, some oxides like ZrO_2 and HfO_2 are fast oxygen conductors. However, formation of MoO_3 was limited to the surface of the I2a specimen with higher density, denying that the particles cause accelerated oxidation in the interior of the sample. Selective oxidation at the surface might result from introducing defects when grinding the sample prior to the test.

At low temperatures the particles could influence the oxidation behaviour in several ways. Since they are oxides themselves (ZrO_2 and HfO_2) or easily develop an oxide scale (SiC), the oxidation rate of the composites should be decreased compared to pure $MoSi_2$. This can be explained as follows: For oxide second phases the affected surface of the composite is decreased ideally by the amount of the second phase, i.e. for the composites described in this paper only 85% of the surface can oxidise, resulting in a lower oxidation rate based on the entire surface. For SiC, oxidation of this phase can result in formation of an oxide scale which seals the surface and prevents further "pest" oxidation. On the other hand, all second phase particles provide additional interfaces, acting as starting points for pesting and increasing the oxidation rate.

Though composites and pure $MoSi_2$ cannot necessarily be compared at a certain temperature because of the dependence on the composition, the resistance to pesting of the pure $MoSi_2$ specimen is most likely due to its high density, since neither oxidation at 400 °C nor the successional one at 500 °C lead to disintegration.

Preoxidation even of series I2 did not completely prevent pesting as planned, indicated by the white spots on the oxide scale after 575 h at 400 °C, see Fig. 16. It is concluded that the incubation time is prolonged by preoxidation, since the material will show accelerated oxidation later. The same was observed for pure $MoSi_2$.

Based on these results the second phase particles have a rather small influence on pesting of $MoSi_2$ composites, but as for pure $MoSi_2$ the microstructure is crucial. High density and preoxidation will provide a higher resistance against pesting.

4.3 Conclusions for $MoSi_2$ composites containing ZrO_2 or SiC

The problems observed in the oxidation of $MoSi_2/HfO_2$ at very high temperatures, i.e. above 1600 °C, like the formation of a liquid phase at 1700 °C can easily be transferred to the composite containing ZrO_2. The eutectic temperature of SiO_2-ZrO_2 is in the same range. Generally, Zr and Hf and their oxides are quite similar.

Since there are no eutectics in the $MoSi_2/SiC$-SiO_2 system, it is assumed that the temperature limit of $MoSi_2/SiC$ is somewhat higher. Silica melts at 1723 °C. However, high amounts of Mo_5Si_3 may lead to bubble formation similar to what had occurred at 1600 °C when testing $MoSi_2/HfO_2$, which is below the eutectic temperature of HfO_2-SiO_2. Evaporation of CO causes bubbles in the silica scale of SiC at

1700 °C [10] and has to be considered in addition to gaseous MoO_3 when testing the $MoSi_2$/SiC composite.

As a general conclusion it may be stated that optimised $MoSi_2$ composites can be suitable for use up to something like 1600 °C (but not for temperatures significantly higher).

5 Acknowledgement

The financial support of these investigations by the Bundesministerium für Bildung, Wissenschaft, Forschung und Technologie (BMBF) (contract number 03 N 2015 C1) is gratefully acknowledged by the authors. Thanks are also due to Ms. Schorr (EPMA), Mr. Gawenda (SEM), and Ms. Berghof-Hasselbächer (metallography).

6 Literature

[1] S. Lohfeld, M. Schütze, Materials and Corrosion 2005, 56, 93.

[2] S. Lohfeld, M. Schütze, Materials and Corrosion 2005, 56, 146.

[3] R. W. Bartlett, P. R. Gage, Transactions of the Met. Soc. of AIME 1965, 233, 968.

[4] S. Melsheimer, Doctoral Dissertation, Technical University of Aachen 1996.

[5] K. Bundschuh, Doctoral Dissertation, Technical University of Aachen 1998.

[6] K. Bundschuh, M. Schütze, Materials and Corrosion 2001, 52, 268.

[7] W. B. Hilling, Mat. Sci. Res. 1987, 20, 697.

[8] ChemSage V4.21, GTT-Technologies, Herzogenrath.

[9] H. Heuschkel, G. Heuschkel, K. Muche (Hrsg.), ABC Keramik. 2. Auflage, VEB Deutscher Verlag für Grundstoffindustrie, Leipzig, 1990.

[10] K. Nickel, P. Quirmbach, In: J. Kriegesmann (Hrsg.): Technische keramische Werkstoffe, Kap. 5.4.1.1, Loseblattsammlung, DKG, 1991.